System Identification and Stability Evaluation of an Unmanned Aerial Vehicle From Automated Flight Tests

Jinyoung Suk*
Department of Aerospace Engineering, Chungnam National University, 220 Gung-dong, Yuseong-Gu, Daejeon, 305-764, Korea
Younsaeng Lee, Seungjoo Kim
UAV Programs, Changwon Plant, Korea Aerospace Industries, Ltd.
Hueonjoon Koo, Jongseong Kim
UAV Team, 3rd System Development Center, Agency for Defense Development

This paper presents a consequence of the systematic approach to identify the aerodynamic parameters of an unmanned aerial vehicle (UAV) equipped with the automatic flight control system. A 3-2-1-1 excitation is applied for the longitudinal mode while a multi-step input is applied for lateral/directional excitation. Optimal time step for excitation is sought to provide the broad input bandwidth. A fully automated programmed flight test method provides high-quality flight data for system identification using the flight control computer with longitudinal and lateral/directional autopilots, which enable the separation of each motion during the flight test. The accuracy of the longitudinal system identification is improved by an additional use of the closed-loop flight test data. A constrained optimization scheme is applied to estimate the aerodynamic coefficients that best describe the time response of the vehicle. An appropriate weighting function is introduced to balance the flight modes. As a result, concurrent system models are obtained for a wide envelope of both longitudinal and lateral/directional flight maneuvers while maintaining the physical meanings of each parameter.

Key Words : System Identification, Unmanned Aerial Vehicle, Automatic Flight Control System, Flight Control Computer, Closed-Loop Flight Test Data

1. Introduction

Modeling of an aircraft forms the basis for stability and control analysis. Accurate modeling precedes the identification of the flight characteristics of the developed aircraft. Basic modeling of an aircraft is obtained at the configuration design stage (Hoak, 1972), which does not reflect all the details of the real configuration. This modeling is sometimes quite different from the real one because the modeling method is largely based on convention or simple experiments. It generally depends on system identification based on flight test data to overcome the discrepancy and obtain an accurate model.

System identification was initiated in 1795 when Gauss developed the least square method to estimate the orbits of planets (Hamel and Jategaonkar, 1996). It was frequently used as a tool to verify and change the mathematical model of various aerospace systems from flight tests. Longitudinal oscillation method, pulse method and analogue matching were developed in the early twentieth century. Estimation theories based on stochastic systems were introduced in the 1960s : output error method, and filter error method, frequency domain identification method were

* Corresponding Author,
E-mail : jsuk@cnu.ac.kr
TEL : +82-42-821-6685; **FAX** : +82-42-825-9225
Department of Aerospace Engineering, Chungnam National University, 220 Gung-dong, Yuseong-Gu, Daejeon, 305-764, Korea (Manuscript **Received** August 26, 2002; **Revised** February 12, 2003)

among them (Iliff, 1989; Jategaonkar and Plaetschke, 1989; Maine and Murray, 1988; Song and Hwang, 1998). Recently, closed-loop identification for statically unstable aircraft and real-time system identification with a controller reconfiguration scheme were pursued (Kuo et al., 2000; Morelli, 1996, 2000; Song et al., 2002).

System identification from flight tests requires a lot of flight data in the whole flight envelope and its results should be consistent with these flight data. In this respect, identification based on aerodynamic parameters is considered better than that based on system and input matrices. Moreover, the aerodynamic parameters to be identified should be constrained within a certain reasonable range. Identification is a kind of optimization in either a deterministic or stochastic environment that consists of (i) selection of performance index, and (ii) optimization that minimizes(maximizes) the selected performance index. It is also a kind of inverse problem that seeks the modeling from the input-output relationship and the desired modeling can be obtained from as many known test data and parameters as possible. That is, the identified modeling reflects the information imposed by the researcher. Therefore, the researcher should apply a consistent flight test method that maximizes the identifiability and uses as much information from either physical insight or wind tunnel tests to minimize the role of the identification algorithm itself.

This paper presents a consequence of the systematic approach to identify the aerodynamic parameters of the developed unmanned aerial vehicle equipped with an automatic flight control system. A brief specification of the unmanned aerial vehicle is shown in Table 1. Programmed actuating inputs that are almost equivalent to the designed trajectories guarantee the highest input frequency attainable. Interference effects between longitudinal and lateral/directional modes should be minimized for accurate system identification, and the desired flight mode was excited while the other flight mode was regulated via autopilot engagement. An enhanced airborne data acquisition system (ADAS) made it possible to get the high-quality flight data (Kim et al., 2001).

Table 1 Specification of the UAV

Description	Value [unit]
Length	4.6 [m]
Span	6.4 [m]
Weight	290 [kg]
Operational Altitude	0-0 [km]
Range	00 [km]
Endurance	0 [hrs]

The flight test data were carefully acquired by considering consistency and reproducibility. The flight data were effectively used for the system identification of the unmanned aerial vehicle. A constrained parameter optimization algorithm was used to find the system model for both longitudinal and lateral/directional flight modes for a large flight speed envelope.

2. Flight Test Strategy

Dynamic response of an aircraft is largely determined by the actuation of control surfaces/propulsion. Therefore, the actuation should be designed in order to excite a wide bandwidth. There has been much research in this area : identifiability was adopted as a performance index and was optimized for the realization of the actuation input. As a result, single pulse, doublet and 3-2-1-1 multistep input were designed and verified via flight tests. Especially, a 3-2-1-1 multistep input was proved efficient with a relatively simple design effort (Klein, 1989; Morelli and Klein, 1990; Morelli, 1997; Schafer, 1984). Fig. 1 shows the configurations and power spectral densities of various actuation inputs with respect to the frequency in Hz.

In this research, a variety of flight tests were performed for system identification taking the advantage of a remotely commanded, automatically controlled UAV. In the longitudinal open-loop flight test, a flight motion was excited by elevator while the throttle was fixed to trim-throttle. In order to decouple the longitudinal mode from the lateral/directional mode, the lateral/directional autopilot was engaged to keep

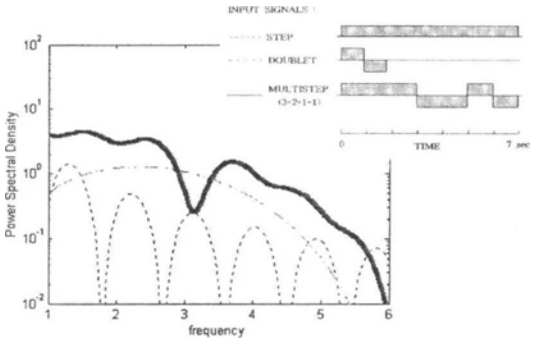

Fig. 1 Frequency domain comparison of various input signals

Table 2 Open-loop flight test results

No	ALT* (m)	IAS** (kph)	Trim Throttle (%)	Weight (Kg)
1	1020	128.7	31.6	265.22
2	1004	150.3	43.6	264.35
3	1010	149.6	41.2	263.88
4	534	129.1	26.0	263.40
5	530	128.4	26.8	263.04
6	518	162.6	42.8	262.25
Roll is regulated by autopilot				

*ALT : Flight Test Altitude
**IAS : Indicated Airspeed

the wing level. Pre-optimized 3-2-1-1 input was automatically excited to guarantee the desired frequency bandwidth (Lee et al., 2001). Several reciprocated flight events were performed within a broad flight envelope to accumulate reliable flight data. The flight data were stored in ADAS with a sample rate of 50 Hz. Such a systematic flight test method contributed to acquiring high quality flight test data. Longitudinal flight tests were performed at the altitude of around 1000 m and 500 m at various airspeeds, which are summarized in Table 2.

On the other hand, additional flight data were obtained from the closed-loop pitch test. The pitch control loop has feedbacks of the pitch angle/angular rate from the integrated navigation unit (INU) and actuates the elevator using the assigned feedback gains. In most UAVs that do not adopt automatic take-off and landing system (ATLS), external pilots control the air vehicle in the take-off and landing phase. Therefore, the pitch control loop requires high bandwidth to increase the recovery rate of the vehicle in accidental situations. Figure 2 shows a block diagram of the pitch control loop. The pitch control loop consists of two individual feedback paths : (i) the pitch tracking error between the pitch command and pitch response, and (ii) the pitch rate. A washout is adopted to remove the nonzero pitch rate during the steady turn. The pitch loop autopilot computes the required elevator command. Actual control surface deflection is an outcome of the servo dynamics, which can be approximated by a

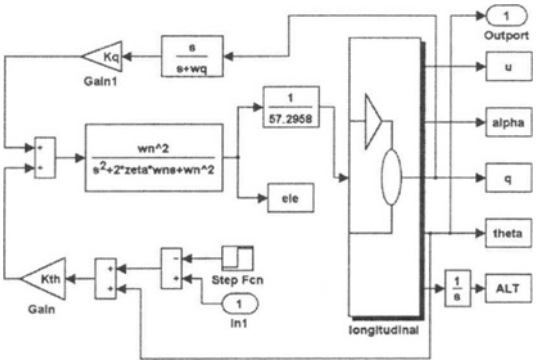

Fig. 2 Pitch loop block diagram

second order transfer function. The output of the longitudinal system is shown at the right end of the figure.

In the closed-loop flight test, a pitch input was used as reference and an elevator was used to follow the pitch command while the throttle was fixed to trim-throttle. Flight data were obtained over a wide speed range. Longitudinal closed-loop flight tests were performed at the altitude of 2000 m at low/high airspeeds as shown in Table 3.

Figure 3 shows one of the test events in Table 3. As shown in the figure, the air vehicle trims near 140 kph and shows the ensuing maneuver after the pitch command of +5 degrees is applied. An offset effect by the aircraft configuration, a pitch response in comparison with the command, the corresponding elevator deflection and reduction of airspeed were detailed in Fig. 3. Aileron

Table 3 Closed-loop flight test results

No	ALT (m)	IAS (kph)	Trim Throttle (%)	Weight (Kg)
1	2004	122.0	55.10	261.78
2	2000	128.2	60.10	261.59
3	1985	142.0	74.00	261.27
4	1992	146.2	70.40	260.87
Roll is regulated by autopilot				

Table 4 Flight test summary (lateral/directional modes)

No	ALT (m)	IAS (kph)	Trim Throttle (%)	Weight (Kg)
1	913	131.0	52.4	273.4
2	910	131.2	53.7	273.1
3	911	130.7	53.1	272.8
4	912	131.3	52.6	272.4
5	914	131.6	52.5	272.1
6	896	160.7	66.3	270.9
7	890	162.0	69.3	270.4
8	894	161.2	67.1	269.9
9	895	162.3	65.9	269.2
10	895	160.0	65.6	268.7
Pitch is regulated by autopilot				

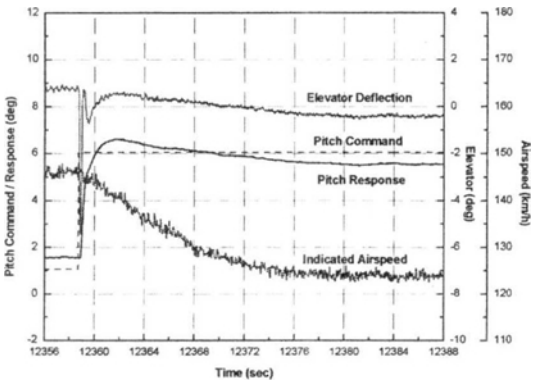

Fig. 3 Closed-loop flight test data

and rudder were used to excite the lateral/directional modes, while the throttle was set to trim-throttle.

The longitudinal mode was regulated by the autopilot as well. A multistep excitation was designed and applied automatically by a preprogram. Stable flight data were obtained for 5 bi-directional test events at both low-speed and high-speed levels. Flight tests were performed at the altitude of around 900 m at low/high airspeeds, which are summarized in Table 4.

3. System Identification

This section deals with the system identification of the air vehicle from the flight data. There have been a lot of literatures on system identification of flight vehicles, however, these can be divided into two categories : (i) MLE (Maximum Likelihood Estimation) and (ii) nonlinear estimation via EKF (Extended Kalman Filter). The former has been studied extensively by Iliff and Maine with a lot of flight data (Iliff, 1989 ; Iliff and Maine, 1984). They have studied the subject for decades, and their study results can be used effectively in the aerodynamic parameter estimation. The MLE scheme is based on maximizing the likelihood function. Consider a dynamic system described by a differential equation with initial conditions :

$$\dot{x}(t)=f[x(t),\ u(t),\ \xi]+F(\xi)\,n(t) \tag{1}$$

$$z(t_i)=g[x(t_i),\ u(t_i),\ \xi]+G(\xi)\,\eta_i \tag{2}$$

$$x(t_0)=x_0 \tag{3}$$

where the discrete time output $z(t_i)$ can be obtained at time t_i, as a function of state vector $x(t_i)$, control input $u(t_i)$, and unknown aerodynamic parameter ξ in addition to the measurement noise. The cost function can be expressed as follows :

$$J(\xi)=\frac{1}{2}\sum_{i=1}^{N}[z(t_i)-\tilde{z}(t_i)]^{*}GG^{*-1}[z(t_i)-\tilde{z}(t_i)] +\frac{1}{2}N\ln|(GG^{*})| \tag{4}$$

where $\tilde{z}(t_i)$ is the predicted response estimate of the states at time t_i, also as a function of unknown parameter ξ. Fig. 4 shows the system identification flow using the MLE scheme.

The method also provides the relative measure of accuracy of the estimated parameters called

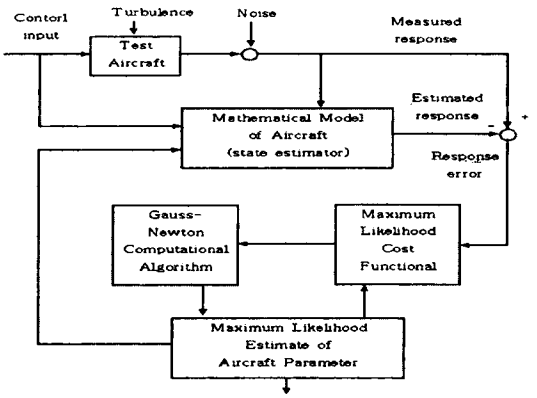

Fig. 4 Maximum likelihood estimation

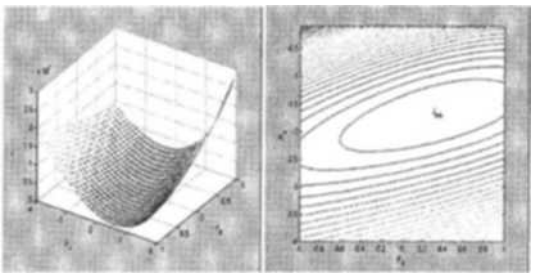

Fig. 5 Performance index variation vis a vis Z_α and Z_{δ_E}

Cramer-Rao bound, which is the square root of the corresponding diagonal element of the information matrix (also known as Hessian). The Hessian matrix can be substituted by a Gauss-Newton approximation in order to improve the convergence and efficiency as follows:

$$H(\xi)=\sum_{i=1}^{N}[\nabla_\xi \tilde{z}_\xi(t_i)]^* G G^{*-1}[\nabla_\xi \tilde{z}_\xi(t_i)] \quad (5)$$

Fig. 5 shows the performance index with respect to two dimensional aerodynamic parameters z_α and z_{δ_E} based on the dynamic equation:

$$z_u u(t)+z_\alpha \alpha(t)+q(t)=z_{\delta_E}\delta_E(t) \quad (6)$$

where z_i means dimensional stability derivatives with respect to i-th states, and $u(t)$, $\alpha(t)$, $q(t)$ and $\delta_E(t)$ denote forward airspeed, angle of attack, pitch rate, and elevator deflection, respectively. Parameters p_4 and p_9 in Fig. 5 mean z_α and z_{δ_E}, respectively. We can see that the performance index is almost the same on a wide range of z_{δ_E}. This sometimes makes the parameters move across the zero-line and converge on a number

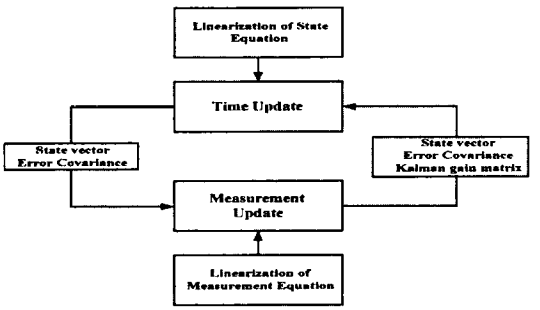

Fig. 6 Extended kalman filter algorithm

that violates the physical meaning. Therefore, we should assign certain bounds on the aerodynamic parameters to be estimated before applying the MLE algorithm. That is often why many MLE/MMLE estimation applications limit the number of parameters to be sought (Kim et al., 1997; Lee and Lee, 1998).

The other method has been applied to the parameter estimation of the aircraft, especially for the guided missile systems (Gelb, 1974; Speyer and Crues, 1987; Song et al., 1995). The method was based on a relatively simple idea and is an extension of the linearization of the conventional Kalman filter to nonlinear problems. In this method, the states should also be estimated as a function of the selected parameters. Besides, the aerodynamic parameters themselves are the ones to be estimated. The EKF algorithms are shown in Fig. 6. Although it can be directly used to the estimation of the aerodynamic parameters, the method is very sensitive to the initial estimates, and in some cases, a discrepancy in initial guess may lead to divergence of the estimation, which is the case for this research.

In this research, a constrained parameter optimization scheme was used to extract the system model based on sequential quadratic programming. The optimization scheme consists of two stages: (i) to select a specific performance index, and (ii) to find the parameters set that minimizes or maximize the performance index. The scheme is in a sense similar to the analog matching method. However, high-performance computer systems and effective search/optimization algorithm substitute the hard working of well-trained parameter tuning engineers. Moreover, the scheme can

be applied to the case where the aerodynamic parameters have constraints, which was impossible in the earlier stage. The optimization procedure assumes deterministic environment. So the flight test data should be of good quality. In addition the following conditions are prerequisites for successful identification.

1. High-performance flight sensors and actuators
2. High-performance flight data acquisition system
3. As many measurements as the number of state variables
4. Reproducible tests at the calm air
5. Consistency of measured flight data

The extracted flight data were preprocessed to filter the measurement noise that undermines the dynamics of the UAV. A second order butterworth filter with a cut-off frequency of 2.5 Hz was used. It is over 5 times the natural frequencies of the short period and dutch-roll mode and it can reject the effect of measurement noise while accommodating both longitudinal and lateral/directional modes. Furthermore, a zero-phase filter was adopted to preclude the effect of phase delay that generally occurs in on-line filtering. Fig. 7 shows the flight data before/after filtering. Zero-phase filtering cannot be applied on-line, but off-line for the research using the post-flight data

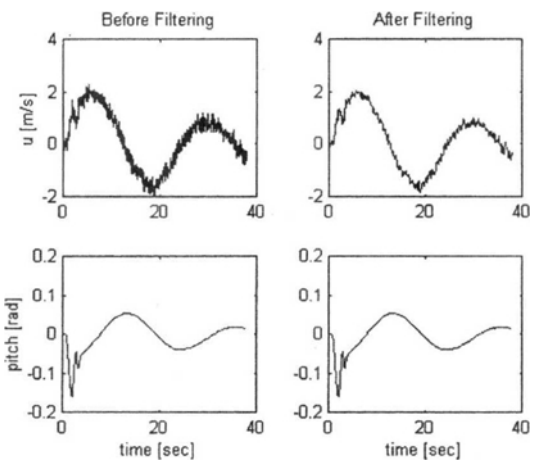

Fig. 7 Flight test data before/after filtering

analysis. Pitch angle history of the vehicle does not show any difference because it is already filtered via INU.

Linear equations of motion of the aircraft system can be expressed as a function of the aerodynamic parameters that are being identified: these are shown in the Appendix. General estimation theory distinguishes the parameter estimation from system variable estimation and two different schemes can be applied for system identification. In the case of aircraft system identification, it would be more efficient to identify via aerodynamic parameters that are almost irrelevant to speed range. In this research, a linear system was derived as a function of the aerodynamic coefficients and the aerodynamic parameters that minimize the error between the estimated system and the real flight data were identified. The performance index was chosen as the weighted error energy between the flight data and numerical responses of the air vehicle when the identical control surface deflection was applied:

$$J=\sum_{i=1}^{4}\kappa_i J_i \tag{7}$$

$$\begin{aligned} J_i &= \| y-y_{est} \|_Q \\ &= \int_{t_0}^{t_f} Q(t)\,[y(t)-y_{est}(t)]^2]\,dt \end{aligned} \tag{8}$$

where J_i, Q, y and y_{est} represent performance indices, their weights, flight data at each test event and responses of the state variables for the linear system model derived from the aerodynamic coefficients. Performance indices for longitudinal mode identification are composed of four (open-loop vs. closed loop, low-speed vs. high-speed) flight test data. Measurements in the open-loop flight test are forward speed (u), angle of attack (α), pitch rate (q), and pitch angle (θ), respectively while those in the closed-loop flight test are u, q and θ. Performance indices for lateral/directional mode identification are composed of four (twice for open-loop, low-speed vs. high-speed) flight test data. Measurements are sideslip angle (β), roll rate (p), yaw rate (r), roll angle (ϕ), and yaw angle (ψ), respectively.

When the performance indices are assigned, all the maneuver modes should be balanced. As

for dynamic response of the longitudinal mode, short-period mode exhibits well-damped high frequency motion while the phugoid mode shows slow motion with very low damping. Therefore, short period motion vanishes in one or two periods after the 3-2-1-1 input is applied and the phugoid mode dominates for the rest of the response. Based on this observation, the following weighting function is chosen so that both short-period and phugoid mode can be considered with the equal proportion :

$$Q(t)=e^{-at}+1 \tag{9}$$

where the effect of phugoid mode can be controlled via the parameter a. A candidate of $a=0.1$ was used in the research. Side constraints were imposed on the aerodynamic coefficients. Static coefficients and others are divided into two groups since the static aerodynamic coefficients are accurate enough from flight tests. While the static coefficients have variations within 10% of their initial values, the others may vary from 10% to 300% of their initial values. Therefore the selected parameters could be optimized to have consistency with the flight data while maintaining the physical concepts. The following equality constraints were applied for control derivatives :

$$C_{m_{\delta E}}=-\frac{l_t}{c}C_{L_{\delta E}} \tag{11}$$

$$C_{l_{\delta R}}=\frac{z_p}{b}C_{y_{\delta R}} \tag{11}$$

$$C_{n_{\delta R}}=-\frac{l_p\cos\alpha+z_p\sin\alpha}{b}C_{y_{\delta R}} \tag{12}$$

where c, l_t, b, z_p and l_p represent mean aerodynamic chord (MAC), horizontal distance between the CG and the aerodynamic center (AC) of the horizontal tail, wing span, vertical distance between the AC of the vertical tail and the fuselage center line and horizontal distance between CG and AC of vertical tail, respectively. In the identification process, other equality constraints were imposed on the steady state response of the pitch loop flight test. Steady state of the air vehicle is given by

$$\left.\frac{\theta}{\theta_c}\right|_{ss}=-\left.\frac{K_\theta G(s)}{1-K_\theta G(s)}\right|_{s=0} \tag{13}$$

where θ_c, K_θ and $G(s)$ represent pitch command, pitch gain, and open-loop transfer function of $\frac{\theta}{\delta E}$ respectively. Open-loop steady state of forward speed can be obtained using the relationship between the closed-loop pitch command and forward speed :

$$\left.\frac{u}{\delta E}\right|_{ss}=\left.\frac{u}{\theta_c}\right|_{ss}\cdot\left.\frac{1-K_\theta G(s)}{K_\theta}\right|_{s=0} \tag{14}$$

Identification results are obtained via an integrated optimization algorithm which blends flight test data and performance indices given by Eqs. (7)-(9) with equality constraints shown in Eqs. (10)-(14) and side constraints for aerodynamic parameters.

4. System Identification Results

A consequence of the system identification procedure and its results are shown in this section.

First, the performance indices [Eqs. (7)-(8)] are constructed from the flight test data and the system response. Weights for each performance index are given by

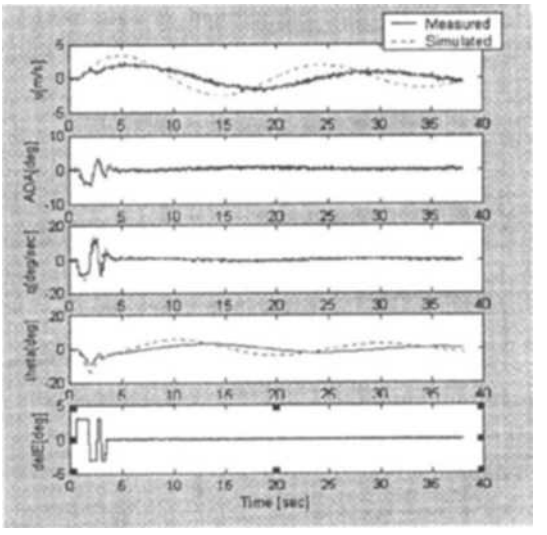

Fig. 8 Flight test data compared with DATCOM modeling (longitudinal)

$$\kappa=[1 \quad 0.1 \quad 0.5 \quad 0.5] \tag{15}$$

In addition, closed-loop steady state response and side constraints for each parameter are included in the optimization algorithm. A mathematical model based on Stability and Control DATCOM was used as an initial guess. Fig. 8 shows the system response using the initial design values. Some discrepancy in phugoid mode is shown in the figure. Tables 5-6 list the estimation of the aerodynamic parameters and dynamic characteristics of the longitudinal motion. Also, an identified linear dynamic modeling is shown in Appendix.

Figures 9-12 show comparative results for the flight test data and numerical simulations using the estimated system dynamics. The sum of C_{m_q} and $C_{m_{\dot{\alpha}}}$ in Table 5 determines the short-period damping, which shows some increase while there is no significant variation in short-period natural frequency depending on C_{m_q}. The parameters C_{m_q} and $C_{m_{\dot{\alpha}}}$ can be estimated indepen dently from (i) the geometric relationship between $C_{L_{\delta E}}$ and $C_{m_{\delta E}}$, and (ii) a priori knowledge of C_{m_α} because the static parameters can be obtained accurately from ground tests and/or analysis.

Table 5 System identification results (longitudinal)

No	Initial Values	Identified Results	Parameters
1	−0.4378	−0.4095	C_{m_α}
2	6.0593	0.3030	C_{L_q}
3	−13.6635	−23.3433	C_{m_q}
4	1.5797	4.7391	$C_{L_{\dot{\alpha}}}$
5	−4.9298	−0.2465	$C_{m_{\dot{\alpha}}}$
6	0.3841	0.2448	$C_{L_{\delta E}}$
7	−1.2389	−0.7896	$C_{m_{\delta E}}$
8	0.0546	0.0582	C_{D_0}
9	0.0375	0.0338	C_{D_α}
10	0.0021	0.0023	C_{L_1}
11	5.4939	4.9445	C_{L_α}

Table 6 Dynamic characteristics (low speed, 1000 m)

Eigenvalue	Damping	Frequency (rad/s)
-3.57e−002+ 2.84e−001i	1.25e−001	2.86e−001
−3.57e−002− 2.84e−001i	1.25e−001	2.86e−001
−2.32e+000− 2.11e+000i	7.41e−001	3.14e+000
−2.32e+000+ 2.11e+000i	7.41e−001	3.14e+000

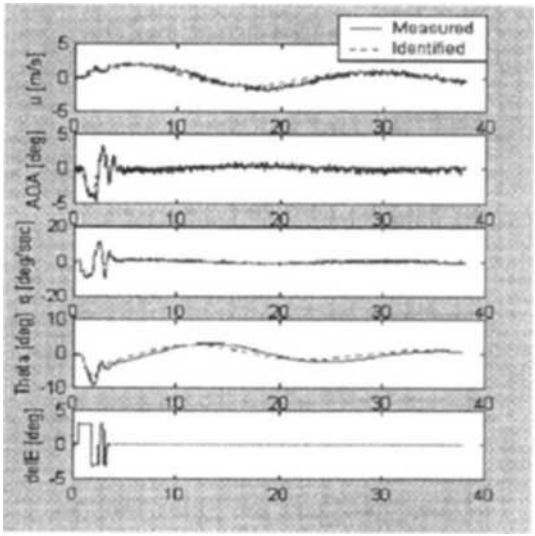

Fig. 9 Longitudinal identification results (open-loop, low speed)

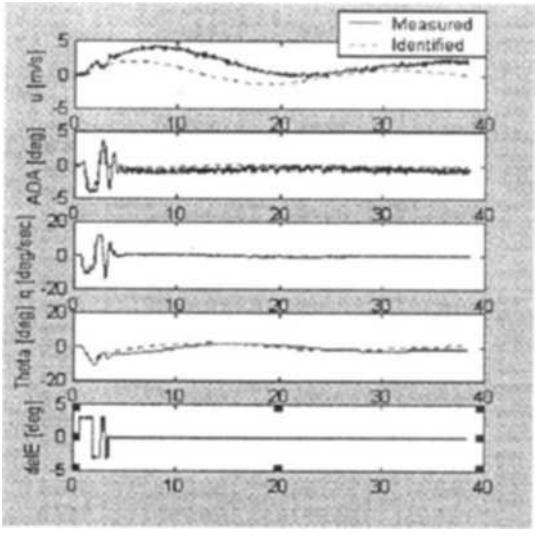

Fig. 10 Longitudinal identification results (open-loop, high speed)

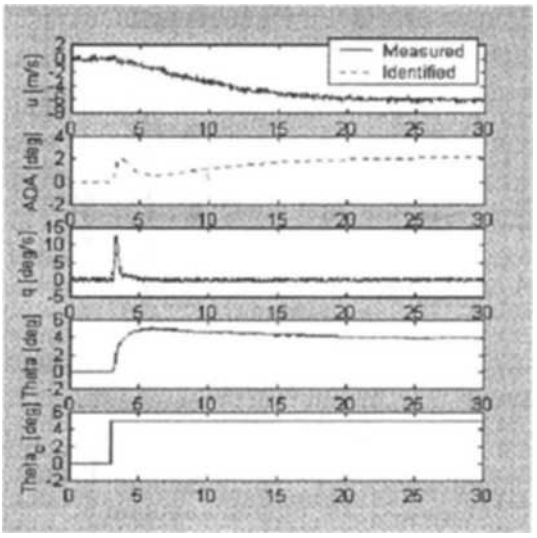

Fig. 11 Longitudinal identification results (closed-loop, low speed)

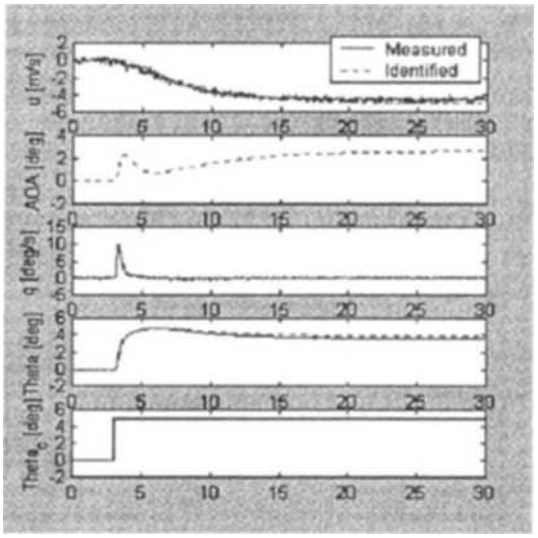

Fig. 12 Longitudinal identification results (closed-loop, high speed)

Besides, initial design results show higher phugoid mode frequency and lower damping than those for the flight tests. The results were reflected in Table 5, where the value of C_{Lq} was lowered to slow the long period motion and the increased drag also increased the long period damping. As shown in the figures, the identified aerodynamic parameters show close responses to those of the flight test data.

Table 7 System identification results (lateral/directional)

No	Initial values		Identified results		Parameters
	low speed	high speed	low speed	high speed	
1	−0.5423		−0.9931		C_{y_β}
2	−0.0296	−0.0391	−0.0047	−0.0180	C_{l_β}
3	0.1150		0.0750		C_{n_β}
4	−0.0944	−0.1090	−0.0096	−0.3270	C_{y_p}
5	−0.5137	−0.5122	−0.3868	−0.4154	C_{l_p}
6	−0.0945	−0.0635	−0.0763	−0.0518	C_{n_p}
7	0.2843		0.6231		C_{y_r}
8	0.2033	0.1520	0.1207	0.1267	C_{l_r}
9	−0.1225	−0.1151	−0.1006	−0.1136	C_{n_r}
10	0.2050		0.1603		$C_{l_{\delta A}}$
11	−0.0212	−0.0151	−0.0015	−0.0021	$C_{n_{\delta A}}$
12	0.1139		0.0976		$C_{y_{\delta R}}$
13	0.0050		0.0043		$C_{l_{\delta R}}$
14	−0.0422		−0.0363		$C_{n_{\delta R}}$

Table 8 Dynamic characteristics (low speed, 1000 m)

Eigenvalue	Damping	Frequency (rad/s)
−5.79e−001+ 2.36e+000i	2.38e−001	2.43e+000
−5.79e−001− 2.36e+000i	2.38e−001	2.43e+000
−5.75e+000	1.00e+000	5.75e+000
7.36e−002	−1.00e+000	7.36e−002

Initial values for lateral/directional identification were derived using DATCOM - a huge database where the stability and control derivatives can be derived for a variety of airfoils and wing-body-tail configurations (Hoak, 1972). Airspeed-dependent aerodynamic parameters were included. Figure 13 shows the system response based on the mathematical model. Yaw rate and sideslip show some discrepancy compared with the flight test data. Tables 7-8 show the identified parameters and resulting dynamic characteristics of the lateral/directional mode. Also, Figures 14-15 show the numerical results from the estimated

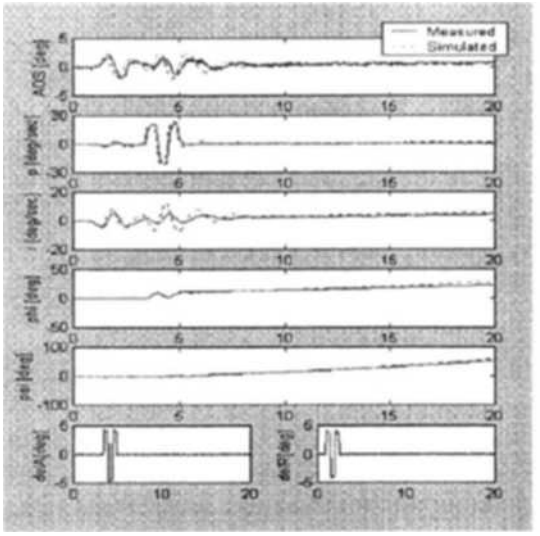

Fig. 13 Flight test datad compared with DATCOM modeling (lateral/directional)

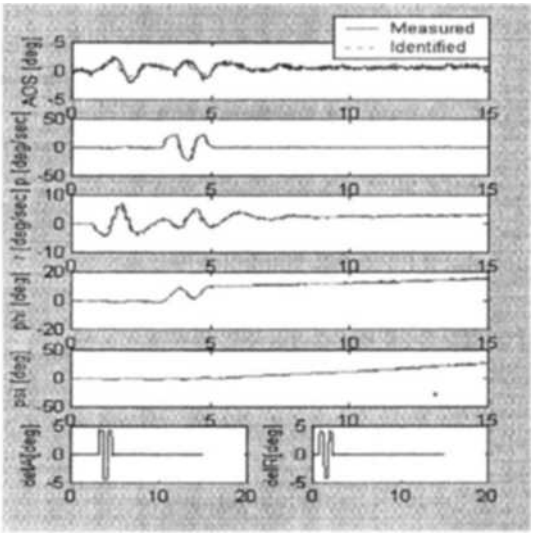

Fig. 15 Lateral/directional identification results (high speed)

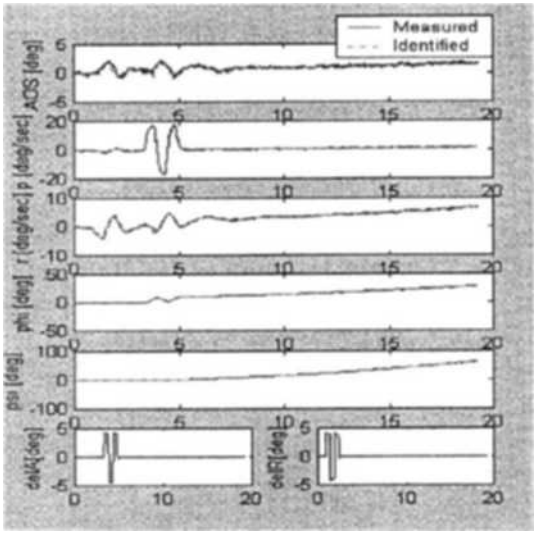

Fig. 14 Lateral/directional identification results (low speed)

dynamics compared with the flight test data. The value of C_{l_r} is estimated to have a lower value than that of the mathematical model in Table 7. The sign of the eigenvalue of the spiral mode is determined by $C_{l_r}C_{n_r}-C_{n_r}C_{l_r}$ and C_{l_r} itself determines the spiral mode dynamics. Therefore, the identified result means that the time to double the amplitude, T_{2s}, for the spiral mode is less in flight tests than that of the mathematical model. Lateral/directional mode dynamics shown in Table 8 explains this. Natural frequency and damping of the dutch-roll mode are quite acceptable. The time constant for the roll mode is kept very low, which indicates good lateral maneuverability. Figures show that the estimated aerodynamic parameters comply well with the flight test results. Table 9 shows the level of flying quality of the developed UAV. Although the UAV will be operating on the autopilot basis, it is designed to guarantee the flight stability so that the external/internal pilots can control the air vehicle manually. Since the international regulation on the stability criteria for UAVs is not well defined, we evaluated the performance referring to the MIL-H-1797 for the aircraft class I, flight phase category B, which is listed in Table 9. As shown in the table, the developed UAV satisfies flying quality level I for the longitudinal mode so that the external/internal pilot can recover the air vehicle manually even in the case of a severe malfunction in autopilot. Especially, the damping of the short period mode is very high, which reflects the high pitch damping in the configuration design stage. Dutch-roll and roll mode of the lateral/directional motion satisfy the flying quality level I while the spiral mode has level II stability. The UAV was designed to have a high-

Table 9 Stability level of the UAV

Flight Mode			Level I Criteria	Test Result	Level
Longitudinal	Short period	$\omega_{n_{sp}}$	$1.11 \leq \omega_{n_{sp}} \leq 6.86$ $(n/\alpha = 14.76)$	3.14	I
		S_{sp}	$0.3 \leq S_{sp} \leq 2.0$	0.74	I
	Phugoid	S_p	$S_p \geq 0.04$	0.13	I
Lateral Directional	Dutch-Roll	ω_{n_d}	$\omega_{n_d} \geq 0.4$	2.43	I
		S_d	$S_d \geq 0.08$	0.24	I
		$\omega_{n_d} S_d$	$\omega_{n_d} S_d \geq 0.15$	0.58	I
	Roll	τ_r	$\tau_r \leq 1.4$ sec	0.17	I
	Spiral	T_{2_s}	$T_{2_s} > 20$ sec	9.42	II

wing type, a long wingspan with a high aspect ratio to guarantee good spiral stability without dihedral. However, the flight test shows spiral stability is not good enough. The composite structure of the wing is found rigid enough to resist upward deflection of the wing in flight.

The evaluation of the flying quality may be of little importance in the sense that the developed UAV is controlled by autopilots in every flight phase and the closed-loop of both longitudinal and lateral/directional modes was designed to guarantee enough stability margins. However, the performance enhancement would be expected via redesign of autopilot gains based on accurate system identification.

5. Conclusions

There is no such identification scheme that meets all the flight test data, and one should apply the estimation method that can best fit to the aircraft considered. This is also quite true for UAVs. UAVs have an advantage in identification flight tests: an automatic flight control system with preprogrammed test modes without further risk increase than manned aircraft. The flight test engineer should take this advantage, and concurrent system identification methods should be applied in order to extract appropriate results. In this research, system identification for both longitudinal and lateral/directional flight modes was performed using the flight test data. Several identification-oriented flight tests were carefully performed. We could estimate the dynamic response of the UAV in a broad range of operational envelope by deriving the equation of motion concurrent with each flight condition and by assigning the aerodynamic coefficients as parameters to be identified. A constrained optimization scheme was adopted for identification : equality/inequality constraints with side constraints were properly used for accurate results. Closed-loop flight tests were implemented to better the accuracy of the identification. As a result of the system identification, dynamic characteristics of the developed UAV were analyzed and the level of flying quality for each flight mode was investigated. The developed UAV was proved to have good flight stability characteristics. The concurrent flight test method with the matched identification algorithm developed in this research can be used for many kinds of UAVs that have programmable test modes equipped with an automatic flight control system.

References

Gelb, A., 1974, *Applied Optimal Estimation*, MIT Press, Cambridge, MA.

Hamel, P. and Jategaonkar, R., 1996, "Evolution of Flight Vehicle System Identification," *Journal of Aircraft*, Vol. 33. No. 1, pp. 9~28.

Hoak, D., 1972 *USAF Stability and Control DATCOM*, Flight Control Division, Air Force

Flight Dynamics Laboratory, Wright-Peterson Air Force Base, Ohio.

Iliff, K. and Maine, R., 1984, *More Than You May Want To Know About Maximum Likelihood Estimation*, NASA-TM-85905.

Iliff, K., 1989, "Parameter Estimation for Flight Vehicles," *Journal of Guidance, Control, and Dynamics*, Vol. 12. No. 5, pp. 609~622.

Jategaonkar, R. and Plaetschke, E., 1989, "Algorithms for Aircraft Parameter Estimation Accounting for Process and Measurement Noise," *Journal of Aircraft*, Vol. 26, No. 4, pp. 360~372.

Kim, H., Kim, Y. and Lee, S., 1997, "Identification Technique of Linear System Using Time Responses and Eigen Information," *Proceedings of AIAA/ASME/AHS Adaptive Structures Forum*, Kissimmee, Florida, USA, April.

Kim, I., Lee, Y. and Suk, J., 2001, "Development of ADAS and Its Verification through Flight Tests," *Journal of the Korean Society for Aeronautical and Space Sciences*, Vol. 29, No. 4, pp. 123~128.

Klein, V., 1989, "Estimation of Aircraft Aerodynamic Parameters From Flight Data," *Progress in Aerospace Science*, Vol. 26, pp. 1~77.

Kuo, C., Schoen, M., Chinvorat, S. and Huang, J., 2000, "Closed-Loop System Identification by Residual Whitening," *Journal of Guidance, Control, and Dynamics*, Vol. 23, No. 3, pp. 406~411.

Lee, H. and Lee, S., 1998, "Parameter Estimation of a Single Turbo-Prop Aircraft Dynamic Model," *Journal of Control, Automation and Systems Engineering*, Vol. 4, No. 1, pp. 38~44.

Lee, Y., Suk, J. and Kim, T., 2001, "Stability Flight Test Methods for an Unmanned Aerial Vehicle," *Proceedings of 2001 Korean Society for Aeronautical and Space Sciences Annual Conference*, Kyongsang National University, Chinju, Korea, Apr. pp. 371~376.

Maine, R. and Murray, J., 1988, "Application of Parameter Estimation to Highly Unstable Aircraft," *Journal of Guidance, Control, and Dynamics*, Vol. 11, No. 3, pp. 213~219.

Morelli, E. and Klein, V., 1990, "Optimal Input Design for Aircraft Parameter Estimation Using Dynamic Programming Principles", AIAA 90-2801 CP.

Morelli, E., 1996, "Parameter Identification Flight Test Maneuvers for Closed Loop Modeling of the F-18 High Alpha Research Vehicle (HARV)," NASA-CR-198269.

Morelli, E., 1997, "Flight Test Validation of Optimal Input Design and Comparison to Conventional Inputs," *Proceedings of AIAA Flight Mechanics Conterence*, New Orleans, Liouisiana, Aug. 11-13.

Morelli, E., 2000, "Real-Time Parameter Estimation in the Frequency Domain," *Journal of Guidance, Control, and Dynamics*, Vol. 23, No. 5, pp. 812~818.

Shafer, M., 1984, *Flight Investigation of Various Control Inputs Intended for Parameter Estimation*, NASA-TM-85901.

Song, C., Jeon, I., Lee, S. and Kwon, S., 1995, "Estimation of the Aerodynamic Parameters for a Flight Vehicle From Flight Test," *AIAA-95-3497-CP*.

Song, Y. and Hwang, M., 1998, "A Study on the Aircraft Parameter Estimation from Flight Test Data," *Journal of The Korean Society for Aeronautical and Space Sciences*, Vol. 26, No. 6, pp. 1~12.

Song, Y., Song, B., Seanor, B. and Napolitano, M., 2002, "On-Line Aircraft Parameter Identification Using Fourier Transform Regression With an Application to NASA F/A-18-HARV Flight Data," *KSME International Journal*, Vol. 16, No. 3, pp. 327~337.

Speyer, J. and Crues, E., 1987, "On-Line Aircraft State and Stability Derivative Estimation Using the Modified-Gain Extended Kalman Filter," *Journal of Guidance, Control, and Dynamics*, Vol. 10, No. 3, pp. 262~268.

Appendix. Flight Dynamic Modeling

1. Longitudinal Equation of Motion

$$\dot{x}(t) = A_{long}x(t) + B_{long}u(t) \tag{A.1}$$

where,

$$x(t) = [u(t) \quad a(t) \quad q(t) \quad \theta(t)]^T, \qquad u(t) = \delta_E(t)$$

$$A_{long} = \begin{bmatrix} X_u = \cos\xi T_u + X_{\dot{a}}\left(\frac{Z_u - \sin\xi T_u}{U_0 - Z_{\dot{a}}}\right) & X_a + X_{\dot{a}}\frac{Z_a}{U_0 - Z_{\dot{a}}} & X_q + X_{\dot{a}}\frac{U_0 + Z_q}{U_0 - Z_{\dot{a}}} & -g\cos\Gamma_0 - X_{\dot{a}}\frac{g\sin\Gamma_0}{U_0 - Z_{\dot{a}}} \\ \frac{Z_u - \sin\xi T_u}{U_0 - Z_{\dot{a}}} & \frac{Z_a}{U_0 - Z_{\dot{a}}} & \frac{U_0 + Z_q}{U_0 - Z_{\dot{a}}} & \frac{g\sin\Gamma_0}{U_0 - Z_{\dot{a}}} \\ M_u = \frac{z_j m}{I_{YY}}T_u + M_{\dot{a}}\left(\frac{Z_u - \sin\xi T_u}{U_0 - Z_{\dot{a}}}\right) & M_a + M_{\dot{a}}\frac{Z_a}{U_0 - Z_{\dot{a}}} & M_q + M_{\dot{a}}\frac{U_0 + Z_q}{U_0 - Z_{\dot{a}}} & -M_{\dot{a}}\frac{g\sin\Gamma_0}{U_0 - Z_{\dot{a}}} \\ 0 & 0 & 1 & 0 \end{bmatrix}$$

$$B_{long} = \begin{bmatrix} X_{\delta_E} + X_{\dot{a}}\frac{Z_{\delta_E}}{U_0 - Z_{\dot{a}}} \\ \frac{Z_{\delta_E}}{U_0 - Z_{\dot{a}}} \\ M_{\delta_E} + M_{\dot{a}}\frac{Z_{\delta_E}}{U_0 - Z_{\dot{a}}} \\ 0 \end{bmatrix}$$

2. Lateral/Directional Equation of Motion

$$\dot{x}(t) = A_{lat}x(t) + B_{lat}u(t) \tag{A.2}$$

where,

$$x(t) = [\beta(t) \quad p(t) \quad r(t) \quad \phi(t) \quad \psi(t)]^T, \qquad u(t) = [\delta_A(t) \quad \delta_R(t)]^T$$

$$A_{lat} = \begin{bmatrix} \frac{Y_\beta}{U_0} & \frac{Y_p}{U_0} & -\left(1 - \frac{Y_r}{U_0}\right) & \frac{g\cos\Gamma_0}{U_0} & 0 \\ \frac{I_{XX}I_{ZZ}}{I_{XX}I_{ZZ} - I_{XZ}^2}\left(L_\beta + \frac{I_{XZ}}{I_{XX}}N_\beta\right) & \frac{I_{XX}I_{ZZ}}{I_{XX}I_{ZZ} - I_{XZ}^2}\left(L_p + \frac{I_{XZ}}{I_{XX}}N_p\right) & \frac{I_{XX}I_{ZZ}}{I_{XX}I_{ZZ} - I_{XZ}^2}\left(L_r + \frac{I_{XZ}}{I_{XX}}N_r\right) & 0 & 0 \\ \frac{I_{XX}I_{ZZ}}{I_{XX}I_{ZZ} - I_{XZ}^2}\left(N_\beta + \frac{I_{XZ}}{I_{ZZ}}L_\beta\right) & \frac{I_{XX}I_{ZZ}}{I_{XX}I_{ZZ} - I_{XZ}^2}\left(N_p + \frac{I_{XZ}}{I_{ZZ}}L_p\right) & \frac{I_{XX}I_{ZZ}}{I_{XX}I_{ZZ} - I_{XZ}^2}\left(N_r + \frac{I_{XZ}}{I_{ZZ}}L_r\right) & 0 & 0 \\ 0 & 1 & \tan\Gamma & 0 & 0 \\ 0 & 0 & \frac{1}{\cos\Gamma_0} & 0 & 0 \end{bmatrix}$$

$$B_{lat} = \begin{bmatrix} \frac{Y_{\delta_A}}{U_0} & \frac{Y_{\delta_R}}{U_0} \\ \frac{I_{XX}I_{ZZ}}{I_{XX}I_{ZZ} - I_{XZ}^2}\left(L_{\delta_A} + \frac{I_{XZ}}{I_{XX}}N_{\delta_A}\right) & \frac{I_{XX}I_{ZZ}}{I_{XX}I_{ZZ} - I_{XZ}^2}\left(L_{\delta_R} + \frac{I_{XZ}}{I_{XX}}N_{\delta_A}\right) \\ \frac{I_{XX}I_{ZZ}}{I_{XX}I_{ZZ} - I_{XZ}^2}\left(N_{\delta_A} + \frac{I_{XZ}}{I_{ZZ}}L_{\delta_A}\right) & \frac{I_{XX}I_{ZZ}}{I_{XX}I_{ZZ} - I_{XZ}^2}\left(N_{\delta_R} + \frac{I_{XZ}}{I_{ZZ}}L_{\delta_R}\right) \\ 0 & 0 \\ 0 & 0 \end{bmatrix}$$

3. Identified Flight Dynamic Modeling

$$A_{long}=\begin{bmatrix} -0.0776 & 6.5416 & 0.0000 & -9.8000 \\ -0.0106 & -1.8686 & 0.9836 & 0.9836 \\ 0.0056 & -6.1595 & -3.1345 & 0.0000 \\ 0.0000 & 0.0000 & 1.0000 & 0.0000 \end{bmatrix} \tag{A.3}$$

$$B_{long}=\begin{bmatrix} 0.0000 \\ -0.0912 \\ -11.9923 \\ 0.0000 \end{bmatrix} \tag{A.4}$$

$$A_{lat}=\begin{bmatrix} -0.3419 & -0.0003 & -0.9811 & 0.2691 & 0.0000 \\ -0.7614 & -5.8589 & 1.8224 & 0.0000 & 0.0000 \\ 5.3382 & -0.4955 & -0.6234 & 0.0000 & 0.0000 \\ 0.0000 & 1.0000 & 0.0000 & 0.0000 & 0.0000 \\ 0.0000 & 0.0000 & 1.0000 & 0.0000 & 0.0000 \end{bmatrix} \tag{A.5}$$

$$B_{lat}=\begin{bmatrix} 0.0000 & 0.0336 \\ 27.6171 & 0.7158 \\ -0.0222 & -2.5798 \\ 0.0000 & 0.0000 \\ 0.0000 & 0.0000 \end{bmatrix} \tag{A.6}$$